Analyst

ROYAL SOCIETY OF CHEMISTRY

PAPER

View Article Online
View Journal | View Issue

Cite this: *Analyst*, 2025, **150**, 1652

Raman spectroscopy as a comprehensive tool for profiling endospore-forming bacteria†

Markus Salbreiter, [a,b] Annette Wagenhaus,[a,b] Petra Rösch [a,b]* and Jürgen Popp [a,b,c,d]

Accurate and reliable bacterial identification at the genus and species levels is essential for effective clinical diagnostics. Pathogens such as *Clostridium perfringens*, *Bacillus cereus*, *Clostridioides difficile*, and *Paraclostridium sordellii* pose significant challenges due to their unique cultivation requirements and developmental traits. Building on our previous work demonstrating the differentiation of vegetative *Clostridium* cells from non-*Clostridium* genera, we now aim to extend this approach to distinguish endospores of the same species. Raman spectroscopy was utilized to develop a comprehensive library of endospore spectra, encompassing both pathogenic and non-pathogenic species. This extensive dataset forms the foundation for advanced analytical capabilities. Chemometric analysis of single-endospore Raman spectra revealed significant discriminatory power across multiple hierarchical levels, facilitating the distinction between vegetative cells and endospores. Furthermore, this method enabled precise genus- and species-level classification of endospores, underscoring its potential for high-resolution bacterial endospore identification. These results highlight the versatility and efficacy of Raman spectroscopy in addressing the challenges associated with the identification of bacterial endospores in diverse clinical and environmental contexts. These findings present the first comprehensive library of endospore Raman spectra, demonstrating that Raman spectroscopy combined with chemometric analysis is a robust and reliable method for differentiating endospores of *Clostridium* species from those of *Bacillus*, *Clostridioides*, and *Paraclostridium*. This approach holds significant promise as a precise diagnostic tool for bacterial endospore identification in clinical settings.

Received 30th January 2025,
Accepted 12th March 2025

DOI: 10.1039/d5an00115c

rsc.li/analyst

Introduction

Under unfavourable conditions such as high temperatures, drought, exposure to chemicals, radiation, or scarcity of nutrients, vegetative cells of the bacilli and clostridia possess the ability to undergo a transformative process known as sporulation.[1] This unique mechanism results in the production of the endospore, a dormant and extremely resistant phase that allows the bacteria to live for thousands of years.[2] Endospores develop high resilience by embedding core macromolecules, enzymes, and metabolites in a dehydrated calcium dipicolinate (Ca-DPA) gel.[3] The Ca-DPA gel is enclosed by a semi-crystalline inner spore membrane, which gives the metabolically inactive spore the ability to withstand external factors including heat, UV and solvents. However, endospores maintain a sensory mechanism, which is triggered by favourable environmental conditions and converts the spore back into a vegetative cell.[1,4,5]

Spores from *Clostridium perfringens*, *Clostridioides difficile* (formerly known as *Clostridium difficile*[6]), *Paraclostridium sordellii* (formerly known as *Clostridium sordellii*[7]), and *Bacillus cereus* can be isolated from diverse environments, including animal gastrointestinal tracts and carcasses, wastewater, lawns, hospital rooms, and soil.[8] Infections by these pathogens typically are initiated upon ingestion of spores, although *C. perfringens* can also enter the body *via* contaminating wounds. Upon sensing small-molecule germinants, spores from these pathogens germinate and outgrow into toxin-secreting vegetative cells.[8] *C. perfringens* is the second most prevalent bacterial cause of foodborne disease in the US and the most common *Clostridium* species linked to gas gangrene.[9–11] Other pathogenic *Clostridium* species include the tetanus causing agent *C. tetani* and *C. botulinum*, which causes botulism.[1]

[a]*Institute of Physical Chemistry and Abbe Center of Photonics, Friedrich Schiller University, Helmholtzweg 4, Jena, Germany. E-mail: Petra.roesch@uni-jena.de; Tel: +49 3641 948381*
[b]*InfectoGnostics Research Campus Jena, Center of Applied Research, Philosophenweg 7, 07743 Jena, Germany*
[c]*Leibniz-Institute of Photonic Technology, Member of the Leibniz Research Alliance – Leibniz Health Technologies, Albert-Einstein-Str. 9, 07745 Jena, Germany*
[d]*Cluster of Excellence Balance of the Microverse, Friedrich Schiller University Jena, 07743 Jena, Germany*
† Electronic supplementary information (ESI) available. See DOI: https://doi.org/10.1039/d5an00115c

Furthermore, medical interest has increased in the designated "superbug" *C. difficile* in the past two decades, which is primarily linked to antibiotic-associated diarrhea.[12,13] *P. sordellii* has been associated with rare postabortion infections, pneumonia, endocarditis, arthritis, peritonitis, and myonecrosis.[14,15] As a result, innovative techniques must be explored and developed for a rapid and reliable detection of endospores of pathogenic bacteria such as *Clostridium*.

One such novel approach is Raman spectroscopy (RS). This method converts the target's vibrational information into spectral information, allowing for identification and characterisation of the microorganism. RS is a cost-effective, quick, and easy-to-use identification approach that is non-destructive, culture- and label-free.[16] RS records a sample's whole biochemical makeup ("spectroscopic molecular fingerprint"), allowing for chemometric evaluation. This allows for the characterisation, differentiation, and identification of bacteria at the species and subspecies levels.[17,18] In a clinical environment, this would be extremely useful for identifying the causal pathogen and making a quick diagnosis.[18]

However, due to their widespread existence in nature, spore-forming bacteria have received increased attention in terms of sporulation,[19,20] germination,[21–23] the structure and content of endospores,[19,24,25] and the evaluation of various inactivation strategies.[26–29] Setlow *et al.* found that the water content of the core, the presence of small acid-soluble proteins (SASPs) associated to the DNA, spore coat proteins, core mineral ions, and dipicolinic acid (DPA) can all impact endospore resilience.[30] Raman spectroscopy has already been used to detect specific cell components, with various research groups focusing on the Raman bands of DPA's calcium complex. Surface enhanced Raman spectroscopy (SERS) has been shown to be a reliable method to detect varying concentrations of Ca-DPA in single spores[31,32] as well as pure Ca-DPA.[33] Raman spectroscopy has also been applied to detect DPA in bacterial samples[34] and to determine the Ca-DPA concentration in single spore samples.[35]

Öberg *et al.* showed that spore metabolic activity and germination of spores of *B. cereus* can be tracked using heavy water and micro-Raman spectroscopy.[23] Calcium dipicolinate, due to its high concentration in bacterial spores, has been effectively detected in single spores using Raman spectroscopy,[36–38] SERS,[31,39–42] UV resonance Raman,[35,43] coherent anti-Stokes Raman spectroscopy[44,45] and confocal Raman spectroscopy coupled with laser tweezers (LTRS).[46–48] LTRS allows for the quantitative assessment of Ca-DPA levels in individual spores,[47] the detection of single spores in aqueous solution without the need for reagents,[46] as well as the monitoring of the kinetics of germination processes.[48] SERS was used to not only monitor the germination kinetics of *Bacillus subtilis* endospores[31] but was also used to monitor the DPA release.[39] Raman imaging has also been employed to monitor, detect and identify spore-forming bacteria and spores.[49,50]

Our previous study demonstrated the ability to accurately differentiate vegetative cells of *Clostridium* from non-*Clostridium* genera, including *Bacillus*, *Clostridioides*, and *Paraclostridium*, across multiple hierarchical levels using Raman spectroscopy combined with chemometric evaluation. Additionally, we demonstrated that cultivation conditions—whether aerobic or anaerobic—significantly influence both the Raman spectra and the subsequent chemometric evaluation. These findings underscore the importance of accounting for cultivation methods when analysing bacterial samples, as they can impact the accuracy and reliability of spectral differentiation and classification.[51]

Building on this foundation, the current study extends the scope by focusing on the same bacterial species while exploiting a key physiological feature—their ability to produce endospores. Endospores, known for their resilience and unique structural properties, present additional challenges and opportunities for precise classification. Previous studies have addressed the question of whether bacterial spores can be detected or monitored. They have identified specific biomarker bands in the Raman spectrum and the germination kinetics from spore to vegetative cell. However, to the best of our knowledge, no one has researched anaerobic spore-forming Clostridia, nor has a comprehensive endospore database been established based on *Bacillus* and *Clostridium* Raman spectra. To address this, Raman spectroscopy, with its sensitivity to molecular composition, is employed to analyse and distinguish the endospores of *Bacillus* and *Clostridium* species, as well as representative strains of *Paraclostridium* and *Clostridioides*. We then used Raman spectroscopy to compile an extensive database of Raman spectra from both pathogenic and non-pathogenic bacterial endospores. Once we had gathered our data, we proceeded to assemble it, carry out chemometric analysis, and create a computed model. Finally, we challenged our model using an independent validation process. This approach not only deepens our understanding of bacterial endospore differentiation but also highlights the potential of Raman spectroscopy in expanding the toolkit for advanced microbial diagnostics.

Materials and methods

Strains and cultivation conditions

A detailed description of each species/strain as well as cultivation condition used within this study is provided in Table S1.† Most of the pathogenic and apathogenic bacteria were either obtained from the German Collection of Microorganisms and Cell Culture GmbH (DSMZ), Braunschweig, Germany, the University Hospital Jena (UKJ), Germany, and the American Type Culture Collection (ATCC), Manassas, Virginia, USA.

All *Bacillus* strains were grown either at 30 °C or at 37 °C (*B. cereus* DSM345 and DSM351) on modified nutrient agar (NA) for 8 to 10 days to promote sporulation. Briefly, the modified nutrient agar was prepared with peptone from meat 5.0 g l^{-1}, yeast extract 2.0 g l^{-1}, meat extract 1.0 g l^{-1}, agar 15 g l^{-1}, and $MgSO_4 \cdot 7H_2O$ 500 mg L^{-1} at pH 7.0.[52]

The *Clostridium*, *Paraclostridium* and *Clostridioides* strains were grown at 37 °C under anaerobic conditions within an

anaerobic incubation system by Anaerocult and using Anaerocult A pads for the generation of an oxygen-deprived environment in an anaerobic jar (VWR, Darmstadt, Germany) for 10 to 14 days to promote endospore production. The BHI agar was prepared with HM infusion powder 12.5 g L^{-1}, brain heart infusion powder 5 g L^{-1}, proteose peptone 10 g L^{-1}, dextrose (glucose) 2 g L^{-1}, sodium chloride 5 g L^{-1}, disodium phosphate 2.5 g L^{-1} and agar 15 g L^{-1} at pH 7.4 ± 0.2. Alternatively, 52 g L^{-1} of completed BHI agar can be dissolved and distributed in Petri dishes after autoclaving at 121 °C for 15 min. Most of the anaerobic strains had to be pre-cultured on Columbia Sheep Blood Agar (VWR, Darmstadt, Germany) before being able to efficiently grow and produce the desired number of endospores on BHI agar.

Furthermore, certain clostridial species such as *C. butyricum* and *C. tertium* were grown on modified nutrient agar (NA) containing 100 mg l^{-1} $CaCl_2{\cdot}2H_2O$ rather than $MgSO_4{\cdot}7H_2O$.[52] Moreover, *C. perfringens* was grown on tryptose sulfite cycloserine (TSC) agar containing enzymatic digest of casein 15 g l^{-1}, soy peptone 5 g l^{-1}, yeast extract 5 g l^{-1}, sodium meta-bisulfite 1 g l^{-1}, ferric ammonium citrate 1 g l^{-1}, cycloserine 0.4 g l^{-1}, egg yolk emulsion 50 ml, and 18 g l^{-1} agar (VWR, Darmstadt, Germany). Alternatively, pre-made Petri dishes are commercially available (VWR, Darmstadt, Germany). All the chemicals used for the media production were bought through VWR (Darmstadt, Germany) and Merck (Darmstadt, Germany).

Sample preparation

The cultured strains were scraped from the plate and put into 1 ml sterile dH_2O-filled Eppendorf tubes (VWR, Darmstadt, Germany). On a case-by-case basis, some strains were suspended for one to three days in 1 ml sterile dH_2O for vegetative cells to lyse and/or release endospores from their mother cells. The cell suspension was then rinsed and centrifuged three times with 1 ml sterile dH_2O at 10 000 rcf for 5 minutes at 4 °C. Next, the pellet was resuspended in 200 µl dH_2O. After taking 10 µl of the solution with an Eppendorf pipette, small droplets were deposited on nickel foil. If the sample was too turbid or the cell count was too high to assess single cells or spores, serial dilutions were used. After the suspension droplets were dried at room temperature on the nickel foil, they were measured by Raman spectroscopy.

Raman measurements

The BioParticleExplorer (BPE4, rap.ID, Berlin, Germany) with a frequency-doubled (532 nm), solid-state diode pumped Nd:YAG laser (LCM-S-11-NNP25, Laser-export Co. Ltd, Moscow, Russia) and an Olympus MPL-FLN-BD 100× objective (Olympus Corporation, Tokyo, Japan) was used to perform Raman spectroscopic measurements of single endospores. The 100× objective focuses Raman excitation light onto the sample with a spot size of less than 1 µm and a laser power of 10 mW. The backscattered Raman light is diffracted using a single-stage monochromator with a 920 lines per mm grating (HE532, Horiba Jobin Yvon, Bensheim, Germany) before being detected using a thermoelectrically cooled CCD (DV 401 BV; Andor Technology, Belfast, UK). As a result, a spectral resolution of about 8 cm^{-1} is provided.

Before measuring the endospore samples, 4-acetamidophenol (4-AAP) was measured for the calibration of the wavenumber axis at 50% laser intensity for 5 s. For each sample 50–60 spectra were obtained in three biological replicates. To make sure that the signal-to-noise ratios are comparable between the bacteria, most of the endospores were measured at 10% laser intensity with an exposure time of 5 s to ensure that the spores do not burst. Moreover, the *B. cereus* spores were more robust and were measured for 5 s with a 25% laser intensity. Additionally, some of the samples had to be measured slightly out of focus to not rupture the spores. Notably, some of the endospores appeared "coffee bean"-shaped.

Data pre-processing

The data analysis of the raw Raman spectra is a critical step since it removes unwanted artefacts and variation within the different spectra, while also enhancing certain key differences between the various bacterial spore spectra. The data pre-processing was performed using the Ramanmetrix software for Raman data analysis containing a vast array of different steps.[53] The first step is the removal of artefacts such as cosmic interferences in form of spikes by cutting off below 350 and above 3150 cm^{-1} as well as the wavenumber axis calibration with the measured spectra of the 4-AAP to correct the peak position and make measurements of different days comparable.[54,55] A sensitive nonlinear iterative peak (SNIP) clipping algorithm was used to make a baseline correction and to remove the fluorescent background.[56] Finally, the silent region from 1800 to 2600 cm^{-1} was cropped and vector normalization was applied before the pre-processed mean spectra were calculated.

Evaluation of the endospores

To compare the mean spectra of the bacterial endospores, a combination of principal component analysis (PCA) and linear discriminant analysis (LDA) was chosen. PCA-LDA models have already been proven to be highly effective models suited for classifying and identifying different bacterial species based on their Raman spectra. Hereby, the number of principal components was optimized to a certain amount and a random N-fold cross validation was performed. For species-level differentiation, principal component analysis (PCA) was combined with a support vector machine (SVM). SVM is a supervised learning algorithm designed for classification, which determines the optimal margin or hyperplane in an *n*-dimensional space (where *n* represents the number of features) to effectively separate data points into distinct categories. To enhance classification performance, the number of features was adjusted according to the specific classification task. The same model was then applied for the validation of the independent test data and identification of independent bacterial strains which were previously not included in the main data set.

Results and discussion

In this study, the bacteria were chosen based upon their ability to produce endospores, phylogenetic relatedness and clinical relevance. Raman spectra of six *Bacillus* and eight *Clostridium* species as well as *ten C. difficile* and one *P. sordellii* strains were acquired. As already mentioned in the materials and methods section, each species was cultivated either aerobically (*Bacillus*) or anaerobically (*Clostridium*, *Paraclostridium* and *Clostridioides*), whereas individual species were cultivated using different media compositions. Additionally, Raman spectra of pure substances relevant to the Raman spectra of the endospores were measured as reference spectra. These reference spectra can be found in the ESI Fig. S1.†

Raman band assignment

The mean Raman spectra from single vegetative cells and endospores of *Bacillus* and *Clostridium* are presented in Fig. 1. The Raman spectra of vegetative cells exhibit the characteristic spectral pattern found in bacterial spectra, exhibiting the whole spectrum of biomolecules.[16,17,57] *Bacillus* and *Clostridium* spectra are comparable in terms of the typical bacterial spectral signals: the C–H stretching vibrations are located at 2933 cm^{-1},[58] whereas the CH_2/CH_3 deformation vibrations are found at 1451 cm^{-1},[59–61] which are primarily found in lipids and proteins. Furthermore, the Raman signals at 1664 cm^{-1} (ref. 62 and 63) and 1250 cm^{-1} (ref. 64) correspond to amide I and amide III vibrations of proteins. Additionally, the ring breathing vibration of phenylalanine is located at 1004 cm^{-1},[61] while the out of plane ring deformation vibration and the second ring breathing mode of tyrosine give rise to bands at 854 cm^{-1} (ref. 64 and 65) and 824 cm^{-1},[27] respectively. Moreover, nucleic acids can be seen at 1583 cm^{-1}.[62,65] Finally, *Bacillus* vegetative cells have unique Raman signals at 1583, 1397, 1313, 1127, and 749 cm^{-1} (ref. 66–68) that correspond to cytochrome vibrations but are absent in *Clostridium* spectra.

In contrast, the endospore spectra revealed unique Raman signals at 1574, 1445, 1397, 1016, 821 and 659 cm^{-1} (ref. 69 and 70) which correspond to the calcium dipicolinate content in the spore core. At 1574 cm^{-1} the skeletal vibration of the pyridine ring is observed, whereas 821 cm^{-1} corresponds to the C–COO– stretching vibration.[69,70] The pyridine ring breathing vibrations can be detected at 1445 cm^{-1} and 1016 cm^{-1}, while 1397 cm^{-1} represents the OCO symmetric stretching vibration.[69,70] Additionally, the aromatic C–H stretching vibration at 3080 cm^{-1} can be attributed to Ca-DPA.[69,70] Ca-DPA also superimposes signals from different biomolecules such as the ring breathing mode of tyrosine at 821 cm^{-1},[64,65] the CH_2/CH_3 deformation mode of proteins and lipids at 1450 cm^{-1},[59–61] as well as the ring vibrations of adenine and guanine at 1574 cm^{-1}.[62,65]

Additionally, the difference spectra in Fig. 2 were derived by subtracting the pre-processed vegetative cell mean spectra from the endospore mean spectra. This was performed once for *Bacillus* and once for *Clostridium*. Both spectra show the unique Ca-DPA Raman signals at 1574, 1445, 1397, 1016, 821, and 659 cm^{-1} on the positive side,[69,70] emphasising the fact that Ca-DPA can only be found in endospores and not in vegetative cells. In addition to the Ca-DPA bands, *Bacillus* vegetative cells exhibited distinct cytochrome marker bands at 1313, 1127, and 749 cm^{-1}.[66–68] However, the cytochrome signals at

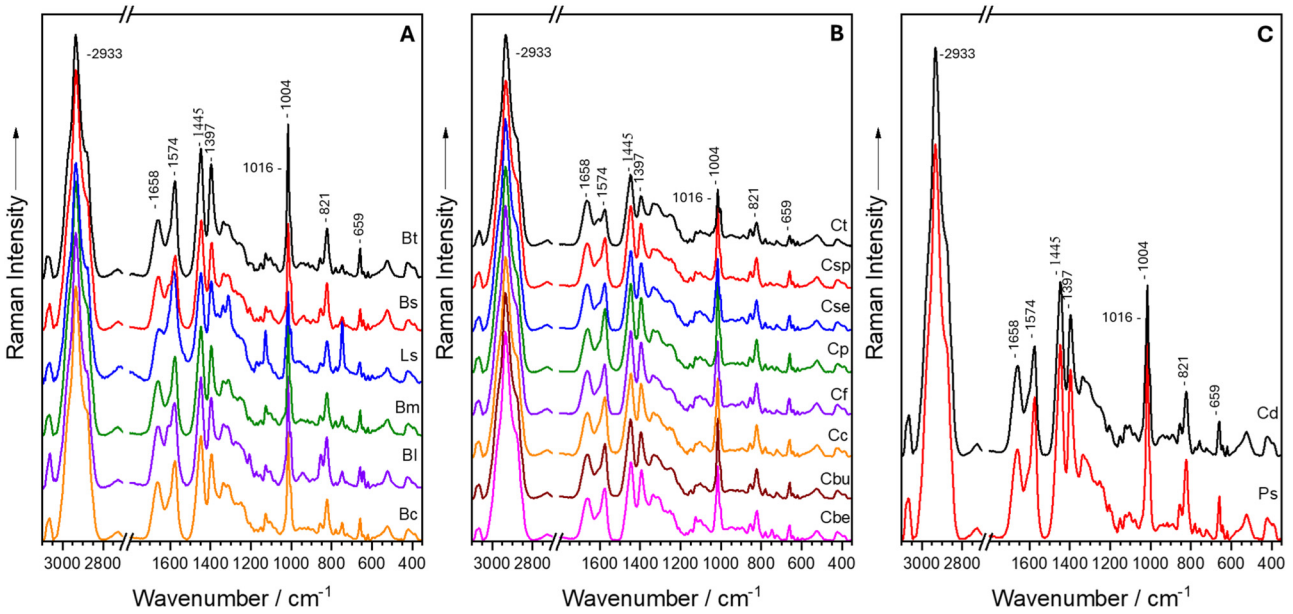

Fig. 1 Mean spectra of endospores of *Bacillus* (A), *Clostridium* (B), *Paraclostridium* and *Clostridioides* (C) species: (Bt) *B. thuringiensis*, (Bs) *B. spizizenii*, (Ls) *L. sphaericus*, (Bm) *B. mycoides*, (Bl) *B. licheniformis*, (Bc) *B. cereus*, (Ct) *C. tertium*, (Csp) *C. sporogenes*, (Cse) *C. septicum*, (Cp) *C. perfringens*, (Cf) *C. felsineum*, (Cc) *C. cadaveris*, (Cbu) *C. butyricum*, (Cbe) *C. beijerinckii*, (Cd) *C. difficile* and (Ps) *P. sordellii*.

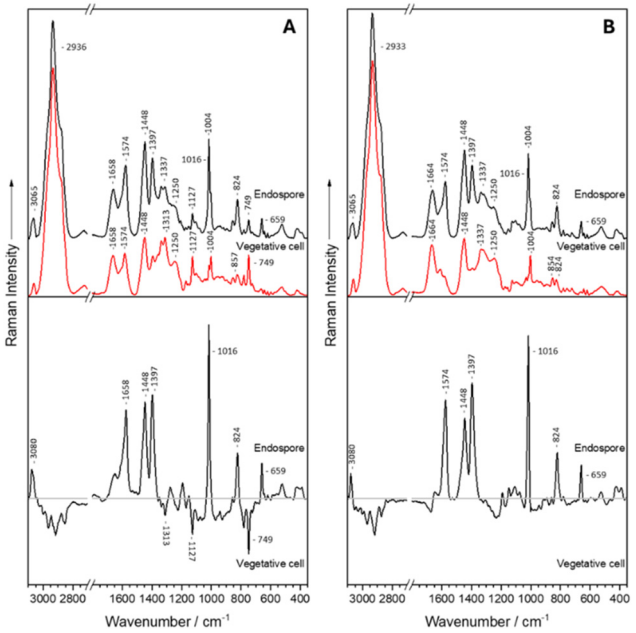

Fig. 2 Mean Raman spectra of endospores and vegetative cells of *Bacillus* (A) and *Clostridium* (B) as well as difference spectra calculated with the mean spectra (endospore – vegetative cell).

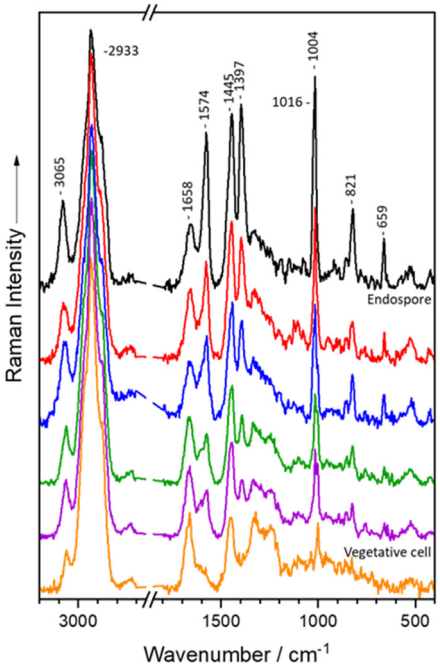

Fig. 3 Raman spectra of single endospore development with increasing Ca-DPA concentration in *C. difficile*.

1583 and 1397 cm^{-1} (ref. 66–68) can not be seen in the difference spectrum for the vegetative cells because they are superimposed by the Ca-DPA signals that arise.[69,70]

Endospore development

Endospore formation, or sporulation, is a tightly regulated developmental process employed by *Bacillus* and *Clostridium* species to endure adverse environmental conditions. This process allows these bacteria to transit from a vegetative state to a metabolically dormant and structurally robust endospore, capable of withstanding extreme stressors such as heat, desiccation, UV radiation, and chemical exposure.

The specific Raman bands associated with calcium dipicolinate (Ca-DPA) arise from the skeletal vibrations of the pyridine ring (659, 1016, 1445, and 3065 cm^{-1}) and the vibrational modes of the carboxylate group (821, 1397, and 1574 cm^{-1}). These characteristic Raman signals serve not only as specific biomarkers for endospores but also as tools to monitor the process of endospore formation, from the initial stages within the mother cell to the release of the mature endospore. It is evident that the mean Raman spectra of different bacterial species exhibit significant similarities, with no distinct marker bands readily identifiable as species-specific (Fig. 1). This highlights the conserved nature of Ca-DPA-related spectral features among endospore-forming species.

Fig. 3 presents individual Raman spectra obtained from different bacterial cells within the same sample, capturing distinct stages of endospore development. These spectra highlight the dynamic changes in both band positions and relative intensities as the bacterial cells transit from a vegetative state (mother cell) to a maturing endospore. Notably, the spectra reveal that the spectral features associated with the vegetative cell differ significantly from those observed in the developing endospore, reflecting the biochemical and structural changes occurring during sporulation. As the endospore matures, there is a marked increase in the incorporation of Ca-DPA, which leads to an enhanced concentration of this compound within the developing endospore. This, in turn, results in a significant intensification of the Raman signal, further emphasizing the key role of Ca-DPA in the maturation process. The progressive evolution of the Raman spectra thus provides a valuable tool for tracking the temporal dynamics of endospore formation, offering insights into the molecular mechanisms underlying bacterial survival in response to environmental stresses.

It is essential to clarify that the Raman spectra presented in Fig. 3 correspond to individually acquired spectra from distinct vegetative cells and endospores, rather than capturing the continuous transition of a single vegetative cell into an endospore. Furthermore, to the best of our knowledge, previous studies have only conducted germination experiments that track the transition from an endospore to a vegetative cell.[21–23]

To determine whether the addition of calcium, manganese, or magnesium during the sporulation process influences the Raman spectra of endospores to a significant extent, *Bacillus cereus* and *Clostridium butyricum* were cultivated on nutrient agar plates enriched with calcium, manganese, and magnesium salts (Fig. 4). This approach allowed for the evaluation of how an addition of these metal ions might affect the biochemical composition and structural properties of the result-

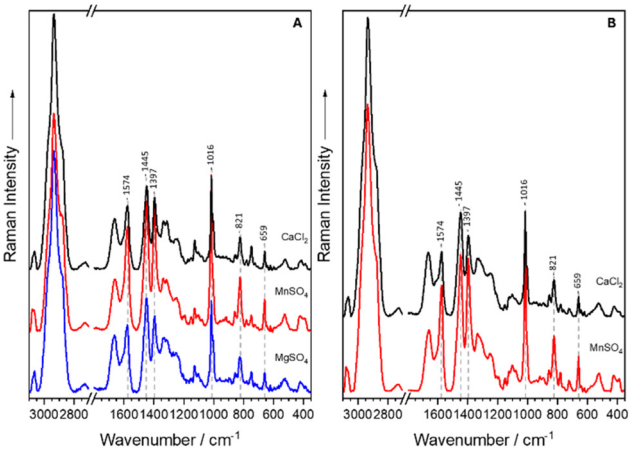

Fig. 4 *Bacillus cereus* (A) and *Clostridium butyricum* (B) were cultured on nutrient agar (NA) supplemented with either $CaCl_2$, $MnSO_4$, or $MgSO_4$.

ing endospores. By comparing the spectra of endospores formed under these enriched conditions to those formed under standard conditions, the aim was to assess any notable alterations in the spectral features that could be attributed to the presence of these additional ions.

A study by Stöckel *et al.*[24] demonstrated the specific effects of supplementary manganese and calcium ions on the Raman spectra of *Bacillus* endospores. In all strains examined, endospores cultivated on manganese-rich agar exhibited a reduction in the intensity of the characteristic Ca-DPA-associated Raman signals at 1016, 1400, and 1572 cm^{-1}. Additionally, band broadening was observed, attributed to the emergence of new bands at 1030, 1390, and 1592 cm^{-1}. This wavenumber repositioning indicates a partial substitution of intracellular Ca-DPA with Mn-DPA, which occurs when spore-forming bacteria are exposed to manganese concentrations significantly exceeding the levels required for vegetative growth.[24]

However, the expected wavenumber variations in the endospore spectra of bacteria grown on calcium- or manganese-supplemented nutrient agar, as reported by Stöckel *et al.*, were not observed in this study. As illustrated in Fig. 4, neither *Bacillus cereus* nor *Clostridium butyricum* grown on agar enriched with calcium, manganese, or magnesium exhibited any significant wavenumber shifts. According to the literature, the stability and formation of metal-ion-DPA complexes are influenced by several factors, including charge density, orbital overlap, ionic radii, solution pH, and the competition and availability of metal ions in the medium.[71] Theoretically, DPA is expected to preferentially bind to Mn^{2+} and Mg^{2+} over Ca^{2+} due to their smaller ionic radii and higher charge densities, which result in the formation of more stable complexes compared to Ca-DPA.[72,73] However, when Ca^{2+} is present in significantly higher concentrations than other metal ions, DPA may bind preferentially to the more abundant calcium despite the lower stability of the resulting complex.[71–74]

The accumulation of metal ions in endospores is primarily influenced by their concentration in the growth medium, though the specific amounts of individual metals can vary significantly. These metals are also partially exchangeable.[75] Among divalent metals, calcium is most closely associated with endospore heat resistance, and its substitution with other metals has been shown to reduce heat resistance.[74,76] The high accumulation of Ca^{2+} in spores may be attributed to its high hydrolytic stability, its relative abundance in standard bacteriological media, and its nontoxic nature.[75] In contrast, Ca^{2+} and Mg^{2+} form chelates with lower stability, making them more prone to dissociation or reversible binding to DPA. Mn^{2+}, while forming more stable complexes, is less easily dissociated, which can lead to biological toxicity.[71,77]

Classification and validation

A more comprehensive evaluation of the Raman spectra was performed using chemometric techniques. Principal component analysis (PCA) combined with linear discriminant analysis (LDA) was applied to distinguish between vegetative cells and endospores, as well as among different genera. PCA is a dimensionality-reduction technique that condenses large data sets into a smaller set of principal components while retaining most of the original information. LDA was then employed for classification and validation, enabling differentiation between the two morphological types and among the genera.

For species-level differentiation, PCA was coupled with a support vector machine (SVM). SVM is a supervised learning method designed for classification, which identifies the optimal margin or hyperplane in an *n*-dimensional space (where *n* is the number of features) to effectively separate data points into distinct categories. The number of features was adjusted based on the classification task to optimize performance. The validation of the training set was performed by using an independent batch of the selected species.

Table 1 summarizes the classification and the validation results for each level (morphology, genus, and species). Initially, a PCA-LDA was employed to discriminate vegetative cells from endospores with an accuracy of 92.9% and sensitivity and specificity of 94.0% and 91.8%, respectively. In this analysis, more vegetative cells were misclassified as endospores (398 out of 4875) than endospores were misclassified as vegetative cells (283 out of 4730). A plausible explanation for this discrepancy could be the varying developmental stages of endospore maturation. The model may struggle to classify partially matured endospores, potentially identifying them as either vegetative cells or endospores with uncertainty.

A genus-level classification was also conducted to evaluate whether endospores from different genera could be reliably distinguished. The dataset included spectra from eight *Clostridium* species, one *Paraclostridium sordellii*, ten *Clostridioides difficile*, and six *Bacillus* species. Of the 4730 endospore spectra analysed, 142 were misclassified. *Clostridium* exhibited the highest misclassification rate with 67 spectra, followed by *Bacillus* and *Clostridioides* with 33 and 34 misclassifications, respectively. *Paraclostridium*, represented

Table 1 Summary of the classification steps on the morphology, genus, and species level

		Classification			Validation		
Level	Name	Acc./%	Sens./%	Spec./%	Acc./%	Sens./%	Spec./%
Morphology	Endospore (ES)	92.9	94.0	91.8	97.7	98.4	97.1
	Vegetative cells (VC)		91.8	94.0		97.1	98.4
Genus	*Bacillus* (B)	97.0	97.1	99.1	93.7	97.8	100.0
	Clostridioides (CS)		97.9	99.6		79.9	99.4
	Clostridium (CM)		96.0	98.6		99.1	93.0
	Paraclostridium (P)		96.8	98.7		96.7	98.4
Species (*Bacillus*)	*B. cereus* (Bc)	97.7	97.0	98.5	87.1	48.0	98.5
	B. licheniformis (Bl)		98.0	100.0		100.0	100.0
	B. mycoides (Bm)		97.1	99.7		82.4	82.8
	L. sphaericus (Ls)		99.2	99.3		100.0	100.0
	B. spizizenii (Bs)		97.7	100.0		100.0	97.3
	B. thuringiensis (Bt)		98.0	99.6		92.0	100.0
Species (*Clostridium*)	*C. beijerinckii* (Cbe)	93.2	88.4	100.0	81.8	93.1	99.8
	C. butyricum (Cbu)		93.8	98.4		100.0	93.3
	C. cadaveris (Cc)		98.6	97.5		100.0	100.0
	C. felsineum (Cf)		90.5	98.8		88.3	93.8
	C. perfringens (Cp)		94.8	99.8		98.3	93.5
	C. septicum (Cse)		87.2	98.6		58.3	97.7
	C. sporogenes (Csp)		97.5	99.8		100.0	100.0
	C. tertium (Ct)		92.3	99.3		16.7	100.0

by only a single species, had the lowest misclassification rate, with 8 out of 250 Raman spectra being incorrectly classified. Thus, the genus-level LDA achieved an overall classification accuracy of 97.0% for the 4730 Raman spectra. Additionally, the model demonstrated sensitivities and specificities ranging from 96.0% to 99.6%, respectively, indicating a robust performance in distinguishing among the genera. The LDA plot (Fig. S2†) further visualizes the discriminatory power of the model, where each dot represents an individual Raman spectrum of one single bacterial cell corresponding to a specific genus.

At the species level, 97.7% of the 1153 *Bacillus* spectra were correctly classified, while the 1688 *Clostridium* spectra were classified with an accuracy of 93.2% (Table 1). Minor misclassifications occurred within the *B. cereus* group (*B. cereus*, *B. licheniformis*, and *B. mycoides*), which are phylogenetically closer to one another than to other *Bacillus* species in the dataset. Additionally, *B. spizizenii* and *B. thuringiensis* occasionally showed misclassifications with *B. cereus*. Notably, *L. sphaericus* achieved the highest classification accuracy, with only one misclassified spectrum. The Raman spectra for this species revealed signs of metabolic activity, such as the presence of cytochrome, suggesting that the endospore might still reside within the mother cell or was not yet fully matured. Despite these challenges, the model exhibited high sensitivities and specificities at the species level, ranging from 97.0% to 100.0%.

For Clostridia, 1573 out of 1688 Raman spectra were correctly classified, resulting in an overall accuracy of 93.2%. Minor misclassifications occurred primarily among *C. beijerinckii*, *C. butyricum*, *C. felsineum*, *C. sporogenes*, and *C. tertium*, which were occasionally misclassified as *C. cadaveris*. In contrast, *C. cadaveris* showed only a single misclassification with *C. felsineum*, *C. septicum*, and *C. tertium*. These errors can be attributed to the close phylogenetic relationships among these species. A more significant misclassification involved *C. septicum*, where 16 out of the 23 misclassified spectra (23/180) were incorrectly assigned to *C. felsineum*.

It is important to note that the position of the endospore within the mother cell can vary significantly between species and even among different strains within the same species. The endospore can either be found in a central, eccentric, subterminal, or terminal position with either swelling the mother cell or not.[78] Additionally, structural variations such as the presence of appendages, an exosporium, or differences in the composition of the endospore cell walls can have a profound impact.[79] These structural differences may influence the Raman spectra by altering the biochemical signals detected, ultimately affecting classification accuracy. Such variability highlights the need for careful consideration of these factors when interpreting Raman spectral data and developing classification models for bacterial endospores. Despite these misclassifications, the results underscore the overall robustness of the method in identifying and classifying Clostridia.

The classification of *Paraclostridium* sordellii and *Clostridioides difficile* on a species-level was not performed, because only one representative of each species was used in this dataset. Additionally, a strain-level classification of the ten *C. difficile* strains was not performed. The detailed classification results can be seen in Table 1 and Tables S3–6.†

Each finalized PCA-LDA and PCA-SVM model underwent a validation process using independently cultivated bacterial species previously included in the training set. The validation dataset comprised the same eight *Clostridium* species, six *Bacillus* species, one *Paraclostridium sordellii* species, and ten strains of *Clostridioides difficile*. Independent batches, defined as biological replicates separately cultivated and excluded from

the training phase, were used to evaluate the sensitivity of the models. The constructed models were applied to predict the classifications of these independent validation sets, with the validation process performed at each classification level. For example, the morphology of the validation set was compared to the morphology classification model, and the same approach was applied for genus- and species-level validation (Table 1). However, species-level validation was not conducted for *P. sordellii*, nor was strain-level validation performed for the ten *C. difficile* strains. This procedure ensured the robustness of the models across different hierarchical levels of classification.

Of the 1159 endospore spectra, 1140 were correctly classified, while 1214 of 1250 spectra were accurately assigned to vegetative cells, resulting in an overall accuracy of 97.7% (Table S7†). At the genus level, validation achieved an accuracy of 93.7%, with *Clostridioides* exhibiting 59 misclassifications as *Clostridium*. Misclassifications among the other three genera were minimal. Sensitivity at the genus level ranged from 96.7% to 99.1%, except for *Clostridioides*, which achieved only 79.9% due to the higher rate of misclassification. Specificities were generally high, ranging from 93.0% to 100.0% (Table S8†). At the species level, validation accuracies were lower, with *Bacillus* achieving 87.1% and *Clostridium* achieving 81.8% (Tables S9–10†). These results highlight challenges in species-level differentiation, likely due to overlapping spectral features among closely related species (Table 1).

Compared to other genera, *Bacillus* achieved a species-level accuracy of 87.1% during validation, which is notably lower than the classification model's accuracy of 97.7% (Table 1). The primary source of misclassification was *B. cereus*, where 52 out of 100 spectra were incorrectly classified as *B. mycoides*. This misclassification aligns with findings from our previous study on vegetative cells of *Bacillus* species,[51] which reported frequent misclassification of *B. cereus* as *B. mycoides* due to their close phylogenetic relationship within the *B. cereus* group. In contrast, *B. mycoides* exhibited only one misclassification as *B. cereus*, but eight misclassifications as *B. spizizenii*. These results underscore the challenge of distinguishing species within closely related groups, particularly the *B. cereus* group.

Clostridium achieved a validation accuracy of 81.8%, nearly identical to the validation performance of *Bacillus*, yet a decreased from its classification model (Table 1). The primary misclassifications involved *C. tertium* being incorrectly classified as *C. butyricum* and *C. septicum* as *C. felsineum*. Notably, *C. tertium* and *C. butyricum* are relatively close in the *Clostridium sensu stricto* phylogenetic tree, which likely explains their misclassification. Consequently, the sensitivity for *C. tertium* dropped significantly from 92.3% to 16.7%, while for *C. septicum*, it decreased from 87.2% to 58.3%. In contrast, *C. butyricum*, *C. cadaveris*, and *C. sporogenes* achieved 100.0% sensitivities, demonstrating robust validation performances for these species. Meanwhile, *C. difficile* and *P. sordellii* were validated only at the genus level since each was represented by a single species in the dataset. Tables S7–10† showed more detailed validation results for each hierarchical level of validation.

This study aimed to establish an extensive Raman spectroscopy dataset for endospores of *Clostridium* and *Bacillus* species, as well as *C. difficile* and *P. sordellii*. Anaerobic bacteria are often overlooked due to the challenges associated with their cultivation, despite their clinical and environmental significance. Notably, Raman spectroscopy proved highly effective in distinguishing these four genera across multiple hierarchical levels, achieving remarkably high classification and validation accuracies.

The method demonstrated the ability to easily differentiate between endospores and vegetative cells and yielded comparable species-level classification results for *Bacillus* and *Clostridium*. This highlights that despite their close phylogenetic relationships, the interspecies and intraspecies differences are pronounced enough to be resolved using Raman spectroscopy combined with appropriate chemometric methods. These findings underscore the critical role of selecting suitable chemometric assessments and model types in advancing the study of these often-underappreciated bacteria.

Conclusion

This study aimed to construct a comprehensive endospore Raman spectra dataset for *Clostridium* and *Bacillus* species, alongside *C. difficile* and *P. sordellii*, which are frequently underrepresented in research due to challenges associated with their phylogenetic relationships, cultivation requirements, and pathogenicity. The dataset was meticulously developed to address these challenges, incorporating samples grown under diverse conditions as well as applying rigorous spectral preprocessing methods and model constructions. Notably, Raman spectroscopy demonstrated high efficacy in distinguishing Clostridia from the recently reclassified former *Clostridium* species, *C. difficile* and *P. sordellii*, despite their close evolutionary relationships. This distinction is critical for both clinical diagnostics and environmental microbiology, where accurate identification of these species can significantly impact treatment strategies and ecological studies.

Moreover, the findings underscore the importance of employing suitable chemometric approaches, such as principal component analysis (PCA) and machine learning classifiers, to extract meaningful patterns from the spectral data. The study also highlights how the choice of model types—linear *versus* nonlinear—can influence classification accuracy, particularly for challenging datasets with overlapping spectral features. This research emphasizes the potential of Raman spectroscopy as a powerful tool for robust differentiation and classification in microbial studies, offering insights into microbial taxonomy, pathogenicity, and environmental distribution. These results pave the way for broader applications of Raman-based techniques in microbiology, fostering advancements in both fundamental and applied research.

Author contributions

Markus Salbreiter: conceptualization, data curation, formal analysis, investigation, methodology, validation, visualization, writing – original draft, writing – reviewing and editing. Annette Wagenhaus: data curation, investigation. Petra Rösch: conceptualization, funding acquisition, project administration, supervision, writing – original draft, writing – reviewing and editing. Jürgen Popp: project administration, supervision, writing – original draft, writing – reviewing and editing.

Data availability

Data, metadata, and a data description file are available on Zenodo at **https://doi.org/10.5281/zenodo.14764655**.

Conflicts of interest

The authors do not have any conflicts of interests to declare.

Acknowledgements

Financial support of the Federal Ministry of Education and Research, Germany (Bundesministerium für Bildung und Forschung (BMBF), Deutschland) in the project FastAlert (13GW0460B).

References

1 M. T. Madigan, K. S. Bender, D. H. Buckley, W. M. Sattley and D. A. Stahl, *Brock Biology of Microorganisms*, Pearson Education Limited, 2022, 16th edn, 2021.
2 L. McKane and J. Kandel, in *Microbiology: Essentials and Application*, 1996, pp. 66–95.
3 K. Johnstone, *J. Appl. Bacteriol.*, 1994, **76**, 17S–24S.
4 A. Keynan and H. Halvorson, in *Spores III*, American Society for Microbiology, Ann Arbor, Mich, 1965, pp. 174–179.
5 *Spore Germination and Outgrowth*, ed. M. Paidhungat and P. Setlow, ASM Press, 2001.
6 P. A. Lawson, D. M. Citron, K. L. Tyrrell and S. M. Finegold, *Anaerobe*, 2016, **40**, 95–99.
7 T. Sasi Jyothsna, L. Tushar, C. Sasikala and C. V. Ramana, *Int. J. Syst. Evol. Microbiol.*, 2016, **66**, 1268–1274.
8 M. C. Swick, T. M. Koehler and A. Driks, in *Virulence mechanisms of bacterial pathogens*, ed. I. T. Kudva, N. A. Cornick, P. J. Plummer, Q. Zhang, T. L. Nicholson, J. P. Bannantine and B. H. Bellaire, American Society for Microbiology, 2016, pp. 567–591, DOI: **10.1128/9781555819286.ch20**.
9 J. E. Grass, L. H. Gould and B. E. Mahon, *Foodborne Pathog. Dis.*, 2013, **10**, 131–136.
10 R. Kiu, J. Brown, H. Bedwell, C. Leclaire, S. Caim, D. Pickard, G. Dougan, R. A. Dixon and L. J. Hall, *Anim. Microbiome*, 2019, **1**, 1–14.
11 R. Kiu and L. J. Hall, *Emerging Microbes Infect.*, 2018, **7**, 1–15.
12 F. Barbut, *J. Hosp. Infect.*, 2015, **89**, 287–295.
13 T. Chopra, *Clostridium Difficile Infection in Long-Term Care Facilities: A Clinician's Guide*, Springer, 2019.
14 D. M. Aronoff, *Anaerobe*, 2013, **24**, 98–101.
15 M. Aldape, A. Bryant and D. Stevens, *Clin. Infect. Dis.*, 2006, **43**, 1436–1446.
16 B. Lorenz, C. Wichmann, S. Stöckel, P. Rösch and J. Popp, *Trends Microbiol.*, 2017, **25**, 413–424.
17 A. Pistiki, M. Salbreiter, S. Sultan, P. Rösch and J. Popp, *Transl. Biophotonics*, 2022, **4**, e202200011.
18 M. Salbreiter, A. Pistiki, D. Cialla-May, P. Rösch and J. Popp, in *Raman Spectroscopy in Human Health and Biomedicine*, ed. H. Sato, J. Popp, B. R. Wood and Y. Ozaki, 2023, pp. 337–410, DOI: **10.1142/9789811264610_0010**.
19 J. De Gelder, P. Scheldeman, K. Leus, M. Heyndrickx, P. Vandenabeele, L. Moens and P. De Vos, *Anal. Bioanal. Chem.*, 2007, **389**, 2143–2151.
20 B. L. Liu and Y. M. Tzeng, *Biotechnol. Bioeng.*, 2000, **68**, 11–17.
21 M. Plomp, T. J. Leighton, K. E. Wheeler, H. D. Hill and A. J. Malkin, *Proc. Natl. Acad. Sci. U. S. A.*, 2007, **104**, 9644–9649.
22 D. Chen, S.-s. Huang and Y.-q. Li, *Anal. Chem.*, 2006, **78**, 6936–6941.
23 R. Öberg, T. Dahlberg, D. Malyshev and M. Andersson, *Analyst*, 2023, **148**, 2141–2148.
24 S. Stöckel, S. Meisel, R. Boehme, M. Elschner, P. Rösch and J. Popp, *J. Raman Spectrosc.*, 2009, **40**, 1469–1477.
25 S. Stöckel, S. Meisel, M. Elschner, P. Rösch and J. Popp, *Angew. Chem., Int. Ed.*, 2012, **51**, 5339–5342.
26 S. Stöckel, S. Meisel, M. Elschner, P. Rösch and J. Popp, *Anal. Chem.*, 2012, **84**, 9873–9880.
27 S. Stöckel, W. Schumacher, S. Meisel, M. Elschner, P. Rösch and J. Popp, *Appl. Environ. Microbiol.*, 2010, **76**, 2895–2907.
28 D. Malyshev, T. Dahlberg, K. Wiklund, P. O. Andersson, S. Henriksson and M. Andersson, *Anal. Chem.*, 2021, **93**, 3146–3153.
29 S. Wang, C. J. Doona, P. Setlow and Y.-q. Li, *Appl. Environ. Microbiol.*, 2016, **82**, 5775–5784.
30 P. Setlow, *J. Appl. Microbiol.*, 2006, **101**, 514–525.
31 J. K. Daniels, T. P. Caldwell, K. A. Christensen and G. Chumanov, *Anal. Chem.*, 2006, **78**, 1724–1729.
32 J. Chan, A. Esposito, C. Talley, C. Hollars, S. Lane and T. Huser, *Anal. Chem.*, 2004, **76**, 599–603.
33 S. E. Bell, J. N. Mackle and N. M. Sirimuthu, *Analyst*, 2005, **130**, 545–549.
34 S. Farquharson, L. Grigely, V. Khitrov, W. Smith, J. F. Sperry and G. Fenerty, *J. Raman Spectrosc.*, 2004, **35**, 82–86.
35 W. Nelson, R. Dasari, M. Feld and J. Sperry, *Appl. Spectrosc.*, 2004, **58**, 1408–1412.
36 A. P. Esposito, C. E. Talley, T. Huser, C. W. Hollars, C. M. Schaldach and S. M. Lane, *Appl. Spectrosc.*, 2003, **57**, 868–871.

37 P. Rösch, M. Harz, M. Schmitt, K.-D. Peschke, O. Ronneberger, H. Burkhardt, H.-W. Motzkus, M. Lankers, S. Hofer and H. Thiele, *Appl. Environ. Microbiol.*, 2005, **71**, 1626–1637.
38 P. Rösch, M. Harz, K. D. Peschke, O. Ronneberger, H. Burkhardt and J. Popp, *Biopolymers*, 2006, **82**, 312–316.
39 D. D. Evanoff, J. Heckel, T. P. Caldwell, K. A. Christensen and G. Chumanov, *J. Am. Chem. Soc.*, 2006, **128**, 12618–12619.
40 J. Guicheteau, L. Argue, D. Emge, A. Hyre, M. Jacobson and S. Christesen, *Appl. Spectrosc.*, 2008, **62**, 267–272.
41 X. Zhang, M. A. Young, O. Lyandres and R. P. Van Duyne, *J. Am. Chem. Soc.*, 2005, **127**, 4484–4489.
42 C. Camerlingo, G. Di Meo, M. Lepore, M. Lisitskiy, A. Poli, M. Portaccio, I. Romano and P. Di Donato, *Sensors*, 2020, **20**, 4150.
43 E. Ghiamati, R. Manoharan, W. Nelson and J. Sperry, *Appl. Spectrosc.*, 1992, **46**, 357–364.
44 N. Coluccelli, G. Galzerano, P. Laporta, K. Curtis, C. L. Lonsdale, D. Padgen, C. R. Howle and G. Cerullo, *Sci. Rep.*, 2023, **13**, 2634.
45 N. Coluccelli, G. Cichelli, P. Laporta and G. Cerullo, *Opt. Express*, 2023, **31**, 23245–23259.
46 C. Xie, J. Mace, M. A. Dinno, Y. Q. Li, W. Tang, R. J. Newton and P. J. Gemperline, *Anal. Chem.*, 2005, **77**, 4390–4397.
47 S.-s. Huang, D. Chen, P. L. Pelczar, V. R. Vepachedu, P. Setlow and Y.-q. Li, *J. Bacteriol.*, 2007, **189**, 4681–4687.
48 L. Kong, P. Zhang, G. Wang, J. Yu, P. Setlow and Y.-q. Li, *Nat. Protoc.*, 2011, **6**, 625–639.
49 K. S. Kalasinsky, T. Hadfield, A. A. Shea, V. F. Kalasinsky, M. P. Nelson, J. Neiss, A. J. Drauch, G. S. Vanni and P. J. Treado, *Anal. Chem.*, 2007, **79**, 2658–2673.
50 A. Tripathi, R. E. Jabbour, P. J. Treado, J. H. Neiss, M. P. Nelson, J. L. Jensen and A. P. Snyder, *Appl. Spectrosc.*, 2008, **62**, 1–9.
51 M. Salbreiter, A. Wagenhaus, P. Rösch and J. Popp, *Anal. Chem.*, 2024, **96**, 15702–15710.
52 E. Bast, *Mikrobiologische Methoden: Eine Einführung in grundlegende Arbeitstechniken*, Springer, 2014.
53 D. Storozhuk, O. Ryabchykov, J. Popp and T. Bocklitz, *arXiv*, 2022, preprint, arXiv.2201.07586, DOI: **10.48550/arXiv.2201.07586**.
54 T. Dörfer, T. Bocklitz, N. Tarcea, M. Schmitt and J. Popp, *Z. Phys. Chem.*, 2011, **225**, 753–764.
55 O. Ryabchykov, W. S. Iwan, J. Popp and T. Bocklitz, *Spectroscopy*, 2022, **37**, 48–50.
56 S. Guo, T. Bocklitz and J. Popp, *Analyst*, 2016, **141**, 2396–2404.
57 S. Stöckel, J. Kirchhoff, U. Neugebauer, P. Rösch and J. Popp, *J. Raman Spectrosc.*, 2016, **47**, 89–109.
58 K. Czamara, K. Majzner, M. Z. Pacia, K. Kochan, A. Kaczor and M. Baranska, *J. Raman Spectrosc.*, 2015, **46**, 4–20.
59 J. M. Benevides, S. A. Overman and G. J. Thomas Jr, *J. Raman Spectrosc.*, 2005, **36**, 279–299.
60 S. Managò, G. Zito and A. C. De Luca, *Opt. Laser Technol.*, 2018, **108**, 7–16.
61 N. Töpfer, M. M. Müller, M. Dahms, A. Ramoji, J. Popp, H. Slevogt and U. Neugebauer, *Integr. Biol.*, 2019, **11**, 87–98.
62 K. Maquelin, C. Kirschner, L. P. Choo-Smith, N. van den Braak, H. P. Endtz, D. Naumann and G. J. Puppels, *J. Microbiol. Methods*, 2002, **51**, 255–271.
63 N. Uzunbajakava, A. Lenferink, Y. Kraan, E. Volokhina, G. Vrensen, J. Greve and C. Otto, *Biophys. J.*, 2003, **84**, 3968–3981.
64 G. Azemtsop Matanfack, A. Pistiki, P. Rösch and J. Popp, *Life*, 2021, **11**, 1003.
65 W. E. Huang, M. Li, R. M. Jarvis, R. Goodacre and S. A. Banwart, *Adv. Appl. Microbiol.*, 2010, **70**, 153–186.
66 Y.-S. Huang, T. Karashima, M. Yamamoto, T. Ogura and H.-o. Hamaguchi, *J. Raman Spectrosc.*, 2004, **35**, 525–526.
67 M. Kakita, V. Kaliaperumal and H.-o. Hamaguchi, *J. Biophotonics*, 2012, **5**, 20–24.
68 T. C. Strekas and T. G. Spiro, *Biochim. Biophys. Acta, Protein Struct.*, 1972, **278**, 188–192.
69 P. Carmona, *Spectrochim. Acta, Part A*, 1980, **36**, 705–712.
70 W. H. Woodruff, T. G. Spiro and C. Gilvarg, *Biochem. Biophys. Res. Commun.*, 1974, **58**, 197–203.
71 L. Chung, K. S. Rajan, E. Merdinger and N. Grecz, *Biophys. J.*, 1971, **11**, 469–482.
72 H. R. Curran, B. Brunstetter and A. Myers, *J. Bacteriol.*, 1943, **45**, 485–494.
73 B. J. Kolodziej and R. A. Slepecky, *J. Bacteriol.*, 1964, **88**, 821–830.
74 M. T. Sinnelä, A. M. Pawluk, Y. H. Jin, D. Kim and J.-H. Mah, *Front. Microbiol.*, 2021, **12**, 744953.
75 R. Slepecky and J. Foster, *J. Bacteriol.*, 1959, **78**, 117–123.
76 W. Murrell, Spore formation and germination as a microbial reaction to the environment, presented at the *Symp. Soc. Gen. Microbiol*, 1961, Vol. 11, pp. 100–150.
77 T. Tang, K. Rajan and N. Grecz, *Biophys. J.*, 1968, **8**, 1458–1474.
78 P. Dürre, *Handbook on Clostridia*, CRC Press, Boca Raton, 1st edn, 2005.
79 P. Vos, G. Garrity, D. Jones, N. R. Krieg, W. Ludwig, F. A. Rainey, K.-H. Schleifer and W. B. Whitman, *Bergey's Manual of Systematic Bacteriology: Volume 3: The Firmicutes*, Springer-Verlag, New York, 2011.